NJC

PAPER

View Article Online
View Journal

Cite this: DOI: 10.1039/c5nj03461b

HMF etherification using NH_4-exchanged zeolites†‡

Katia Barbera,[a] Paola Lanzafame,*[a] Siglinda Perathoner,[a] Gabriele Centi,[a] Massimo Migliori,[b] Alfredo Aloise[b] and Girolamo Giordano[b]

Received (in Montpellier, France) 16th December 2015,
Accepted 8th February 2016

DOI: 10.1039/c5nj03461b

www.rsc.org/njc

The properties of BEA, MFI and Silicalite-1 zeolites in the ammonium and protonic forms are studied in the etherification of HMF (5-hydroxymethylfurfural) in anhydrous ethanol and compared with FTIR data on ammonium ion siting and displacement by competitive adsorption, as well as data on ammonium ion dissolution in aqueous solution. For the first time it is demonstrated that ammonium-exchanged zeolites are active and show better performances (particularly for the BEA structure) in the acid-catalyzed etherification reaction. This behavior is associated to a reversible dissociation of NH_4^+ ions, which is favored by the BEA zeolite structure. A critical condition for enhanced catalytic performances is that dissociated ammonia remains in the zeolite cages, and may be reversibly re-adsorbed. It is thus likely that the dissociated ammonia participates in the reaction or induces a confinement effect.

1. Introduction

Zeolites, in addition to their pivotal role as heterogeneous catalysts in acid-catalysis for the production of high quality fuels and chemicals,[1] find increasing applications in biomass transformation reactions.[2–5] The increasing number of papers focused on the use of zeolites for the conversion of biomass derivatives[6–14] shows that these materials will play a determining role in the future of bio-refinery.[15–19] However, the characteristics of biomass platform molecules (rich in oxygen) and the operation conditions (typically in the liquid phase) are rather different from those required for refinery applications (still the main use of zeolites). It is thus necessary to extend the concepts of the use of zeolites beyond the current uses which are essentially related to their acid-properties (Brønsted and, to a minor extent, Lewis acidity) when other transition metals are not present.

One concept not explored is the use of the NH_4-exchanged zeolites. These materials represent the intermediate typically used in preparing the acid form by thermal decomposition. In high-temperature applications, as typically occurs for oil-refinery uses, they are not stable, but for liquid phase operations in mild conditions, as often encountered in biomass platform transformations, they can be potentially utilized. We were thus interested in investigating this new area of the catalytic chemistry of zeolites.

In previous publications[20,21] we reported the performance of mesoporous zeotype materials (Al-MCM-41, SBA-15) on the etherification of HMF with ethanol to produce biodiesel components, demonstrating the important role of the nature, strength and localization of acidic sites in the products selectivity. More recently,[22] the activity of Silicalite-1 (MFI structure) was studied in the same reaction and the role of the surface acidity induced by defects was highlighted. Weak acid sites associated to zeolite defects (hydroxyl nests) were shown to be active in the etherification reaction, a reaction that is of more general interest for zeolites applied to sustainable chemistry/energy topics, from the formation of dimethylether (DME) from methanol[23] to the formation of various additives for fuels.[24,25]

A general dilemma for these reactions is that strong acid sites would enhance the performance but at the same time catalyze secondary reactions. Blocking strong acid sites with a molecule forming a stable, but reversible complex, could be a way to control the acidity and accessibility of these strong sites, in a somewhat similar way to the reversible blocking of very reactive sites in enzymes being one of the key characteristics of the enzyme itself. In liquid-phase acid-catalyzed reactions, the ammonium form of a zeolite can thus enable control and tune the catalytic performance, but this aspect, as mentioned, was never reported in the literature. The etherification of HMF with ethanol, besides its applicative interest,[26,27] is a good model reaction to investigate this aspect of zeolite reactivity due to the strong dependence of the selectivity and catalytic behavior on the acidity.

It may be observed that the catalytic behavior associated to the modification of the intrinsic reactivity of the zeolite active sites by counter-ions was never investigated in detail, although there is emerging evidence for cooperative effects between

[a] University of Messina, Section Industrial Chemistry, ERIC aisbl and CASPE-INSTM, V.le F. Stagno d'Alcontres 31, 98166 Messina, Italy. E-mail: planzafame@unime.it
[b] Department of Environmental and Chemical Engineering, University of Calabria, via Bucci, 87036 Rende, Italy

† Paper dedicated to a friend, François Fajula, in recognition of his pioneering contribution to the advances in zeolite science and technology.

‡ Electronic supplementary information (ESI) available. See DOI: 10.1039/c5nj03461b

framework and extra-framework sites as well as transition state confinement being involved in determining the acidity of zeolites.[28–30] However, a more complex catalytic chemistry is present. We observe that the charge-balancing extra-framework cations occupy well-defined crystallographic positions, exposed at the surface of the intra-crystalline cages and channels where they can act as active centers. Moreover, they are the main sources of intra-zeolitic electric fields, whose strength depends on the cation radius and charge. Their properties, and the electrostatic fields they generate, render the counterions capable of forming adducts with molecules moving inside the framework, resulting in a strong electronic perturbation of the adsorbed molecules and finally in their chemical activation. In proton-exchanged zeolites, bridging Si(OH)Al groups confer a remarkable Brønsted acidity to the framework.[31] These species can form hydrogen-bonded adducts with molecules trapped inside the zeolite voids in appropriate conditions. Such adducts can further evolve to protonated species. The formation of hydrogen-bonded precursors and protonation are usually the first stages of Brønsted acid-catalyzed chain reactions, which, together with shape selectivity, make zeolite heterogeneous catalysts of paramount importance in petrochemistry. The local environment of both Lewis and Brønsted acidic centers affects not only their availability to reactants, but also the stabilization of reaction intermediates/transitional states. The presence of a cation such as NH_4^+, which may reversibly dissociate to NH_3 and H^+, further influences this intra-crystalline reactivity of zeolites, thus offering a better pathway to develop new selective routes on one hand, and to understand this chemistry on the other hand.

There are thus many relevant motivations to investigate the catalytic chemistry of NH_4^+-exchanged zeolites, which go beyond the interest for the specific reactions and catalysis itself, because they represent other elements in understanding the supramolecular chemistry in the void-space of zeolites.[32] To contribute to this knowledge, we report here the role of cationic species (NH_4^+ and H^+) in two tridimensional zeolites (BEA and MFI) having a similar Si/Al ratio. In fact, it is important to compare the behavior of NH_4^+-exchanged zeolites with that of the corresponding acid forms, to better determine the role of the ammonium ion on the catalytic performances. For the same reason, it is important to analyze the effect of zeolite cages with different sizes, being reasonable that a confinement effect would be present in this dynamic equilibrium between the dissociated and un-dissociated ammonium ion forms. MFI is a 10-member ring zeolite, while BEA is a 12-member ring zeolite. Both zeolites have a tridimensional pore structure, but they present different channel dimensions, 0.47×0.46 nm for MFI and 0.59×0.59 nm for BEA. The catalytic performances for the above cited reaction using these two types of zeolites (with comparable Si/Al ratios) were compared and *in situ* techniques were used to investigate the dynamic equilibrium of NH_4^+ in aqueous media. In order to clarify the role of the zeolite structure in relation to the presence of strong acid sites (related to aluminum substitution of Si ions in the zeolite framework), a Silicalite-1 zeolite, *i.e.* with the MFI structure, but without aluminum, was also utilized. In this sample, the acidity is related primarily to defects in the structure.

2. Experimental

2.1 Materials

BEA and ZSM-5 (MFI) zeolites in the ammonium form were provided respectively by Zeolysts Int. (CP814E*) and Alsi Penta (SM-27). The Silicalite-1 sample (NH_4-Sil) was obtained from the synthesized Na-Silicalite-1[22] after treatment with an aqueous solution of NH_4NO_3/NH_4OH (pH = 10.5) to ion-exchange Na^+ with NH_4^+. To generate the acidic forms, each NH_4-form sample was calcined in air with the following temperature program: ramp 2 °C min^{-1} to 500 °C, hold the isotherm for 5 h and then cool down to room temperature. We denote the resulting acidic forms as H-MFI, H-BEA, and H-Sil. For BEA and MFI type zeolites the SiO_2/Al_2O_3 ratio ranges from 22 to 25.

2.2 Catalyst characterization

FTIR measurements of all calcined samples were carried out on self-supporting wafers and the spectra were collected at a resolution of 4 cm^{-1} with a Bruker Equinox 55FTIR spectrophotometer equipped with a MCT detector. The self-supporting wafers were prepared and activated under vacuum (10^{-4} Torr) for 1 hour at 400 °C in an IR cell allowing *in situ* thermal treatments, and a basic probe molecule dosage (acetonitrile, D_3-acetonitrile, D_2O, and pyridine). Then samples were outgassed both at room temperature and 150 °C in order to evacuate the physisorbed molecules.

Strong Lewis and Brønsted acidic site quantification was performed by integrating the area underneath the bands at 1450 and 1545 cm^{-1} after pyridine dosage. The integrated molar extinction coefficients (IMEC) were calculated, according to Beer's law, by dosing pyridine at increasing concentrations into each sample under study after evacuation at 150 °C under high vacuum, as described elsewhere.[22]

A high performance ammonia ion selective electrode (ISE) from Thermo Scientific Orion was used to accurately determine the dissolved ammonia in aqueous solution due to NH_4^+ release from the zeolites. For each experiment, the electrode was immersed in a solution containing 34 mL of distilled water, 680 μL of Ionic Strength Adjuster (ISA) and 1 g of NH_4-zeolite; then ammonia release was monitored in the temperature range 25–50 °C, and in isothermal conditions at 50 °C for 3 hours. Prior to the experiment, the electrode response was calibrated using NH_4^+ standard solutions at the different working temperatures in the range 25–50 °C.

2.3 HMF etherification reaction

The HMF etherification with ethanol was carried out in a Parr autoclave reactor (Teflon-lined) provided with a Parr 4848 controller. Reaction tests were carried out at 140 °C for 30 min, and 1, 3 and 5 h under autogeneous pressure, strictly following the procedure described elsewhere.[22] The reaction products of interest, 5-(ethoxymethyl)furan-2-carbaldehyde (EMF) and ethyl 4-oxopentanoate (EOP) were quantified by GC-FID analyses. The H_2O formation during the catalytic tests was monitored using a Methrom 831 KF Coulombometer instrument at room temperature.

3. Results and discussion

3.1 Catalytic results and comparison with zeolite acidity

In the reaction conditions used for the catalytic tests (140 °C, autogeneous pressure, ethanol as reactant and reaction medium), the main reaction products obtained were EMF and EOP, while other by-products, such as 2,5-furancarboxaldehyde, 2,5-dimethylfuran, 5-(methyl)furan-2-carbaldehyde, ethyl formate, ethyl acetate and diethyl ether, were detected in trace amounts. Attention was focused on EMF and EOP formation, both deriving directly from HMF conversion on Lewis and Brønsted acid centers, respectively. Moreover, the formation of water (see ESI‡), produced *in situ* by ethanol condensation, was observed as already assessed for similar systems.[20] The catalytic behavior of the two zeolites with different topologies (BEA and MFI) in the corresponding NH_4^+ and H^+ forms was followed, and their performance was compared with those of the NH_4^+ exchanged and H^+ Silicalite-1 materials as references for an Al-free MFI structure (Table 1).

All systems show a high productivity in EMF and EOP, with total HMF conversion after 5 h of reaction observed only for NH_4-BEA, H-BEA and H-MFI. This catalytic behavior is in agreement with that observed previously in similar systems,[21,22] where a trend of EMF and EOP formation was demonstrated with the relative amount of Lewis and Brønsted acidic sites, detected after pyridine desorption at 150 °C (close to the reaction temperature), respectively, as reported in Table 2.

The space-time yield to EMF is slightly higher in the ammonium form for BEA and Silicalite-1 than the corresponding H^+ forms, while for MFI it shows an opposite trend. The space-time yield to EOP is decreased in NH_4-exchanged zeolites with respect to protonic form, while nearly constant in Silicalite-1 samples (Table 1).

Table 1 Comparison of catalytic activity for all the samples after 5 hours of reaction. T = 140 °C, HMF = 2.5 mmol, EtOH = 3.4 mL

Samples	HMF conversion (%)	Space-time yield (mmol h^{-1} g_{cat}^{-1})	
		EMF	EOP
NH_4-BEA	100	3.52	0.44
H-BEA	100	3.11	0.62
NH_4-MFI	60	1.29	0.44
H-MFI	100	2.28	0.63
NH_4-Sil	55	0.92	0.15
H-Sil	51	0.82	0.13

Table 2 Amount of strong Lewis (LAS)/Brønsted (BAS) acid sites for all the samples after pyridine desorption at 150 °C

Samples	FT-IR pyridine adsorption (μmol g_{cat}^{-1})	
	LAS[a]	BAS[b]
NH_4-BEA	265	741
H-BEA	274	744
NH_4-MFI	78	758
H-MFI	169	837
NH_4-Sil	5.5	0.36
H-Sil	4	0.17

[a] Calculated using band at 1445 cm^{-1}, 150 °C. [b] Calculated using band at 1545 cm^{-1}, 150 °C.

The analysis of the selectivities to products at 50% of HMF conversion, and in kinetic regime, allows to provide further indications on the differences in specific reactivity of active sites (Fig. 1). The ammonium exchanged forms of all zeolites are more selective toward EMF production than the corresponding protonic form. These differences are more pronounced at least for the more active and selective BEA-type zeolites. There is thus a complex behavior, which cannot be related only to zeolite structure but may depend on a dissociative equilibrium of the NH_4^+ ion. The characterization of the acidity for the NH_4^+ zeolites didn't show substantial differences in terms of the number and strength of acidic sites (Table 2). It should be remarked that pyridine may compete with ammonia for chemisorption on the acid sites of NH_4^+-exchanged zeolites. While this is what likely happens in BEA, only some NH_4^+ is shifted in NH_4-MFI, indicating that some of these sites (particularly Lewis-acid type, LAS) are located in zeolitic pockets that are not accessible to pyridine and probably also HMF.

3.2 Measurement of the concentration of NH_4^+ released in water solution

In order to measure the amount of NH_4^+ ions released in solution, specific tests were performed. The determination of the NH_4^+ ions released directly during the catalytic tests was not possible under the reaction conditions (140 °C and anhydrous ethanol as solvent) because the membrane used in the ion-selective electrode works only in aqueous media. These tests were performed by suspending the NH_4^+ forms of the BEA, MFI and Silicalite-1 zeolites in water and analyzing the amount of NH_4^+ ions released in the solution with an ion-selective electrode in the range 25–50 °C. This type of measurement thus provides an indication of the relevance of this effect, although under different conditions to the catalytic tests because water is formed during the reaction (at the end of reaction is typically in the order of thousands of ppm, see ESI‡).

Fig. 2a shows the variation in the values of the potential (proportional to the NH_4^+ concentration in solution) of the electrode (reported in mV) monitored during the experiments at different working temperatures. The value of the potential of NH_4-Sil is positive (corresponding to a very low NH_4^+ concentration in the solution, about 20 ppm) for the full temperature range studied, indicating a negligible presence of NH_4^+ in the aqueous solution. For NH_4-BEA and NH_4-MFI the potential values are always in the negative range, but two different trends could be observed. A progressive decrease of the potential was observed for both zeolites in the 25–40 °C temperature range, but for NH_4-BEA the initial value of the potential (−35 mV, corresponding to ~1000 ppm of NH_4^+ released in solution) reaches an inflection point at around 45 °C and returns to the initial value at 50 °C. NH_4-MFI shows instead a constant reduction in potential for the entire investigated temperature range, starting from −65 mV (corresponding to 2500 ppm). Within the limits of the extrapolation of the results to higher temperatures and the use of ethanol as solvent, it may be first concluded that there is no relationship between the dissociation constant of the

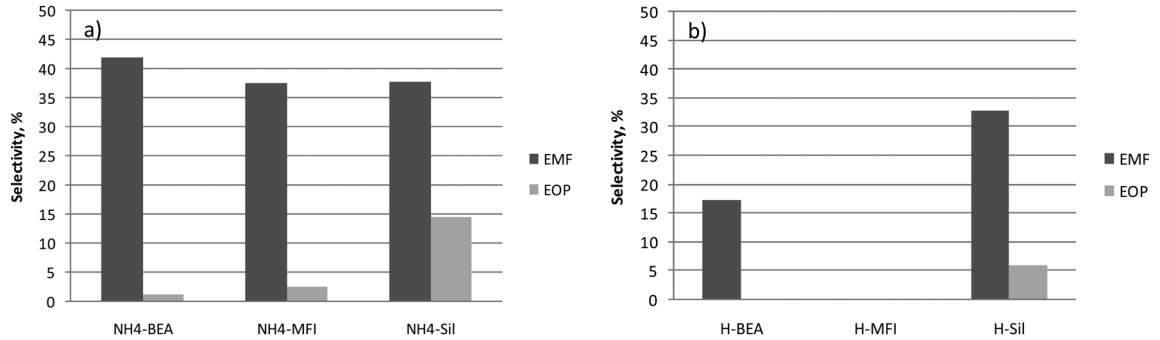

Fig. 1 Product selectivity distribution obtained at 50% HMF conversion for (a) NH_4-series and (b) H-forms. Reaction conditions: T = 140 °C, HMF = 2.5 mmol, EtOH = 3.4 mL.

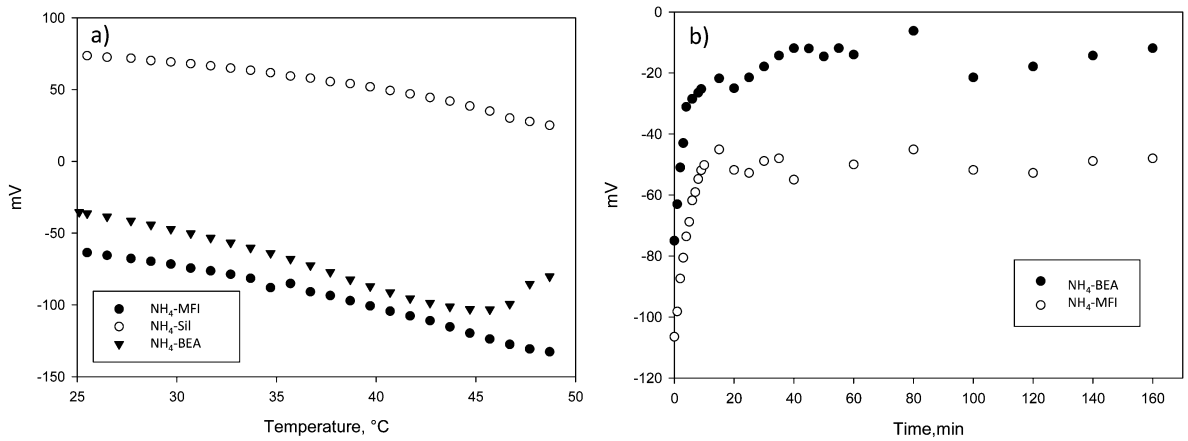

Fig. 2 Variation of NH_4^+ concentration, expressed as mV for the different samples in (a) the T range 25–50 °C and (b) under isothermal conditions: T = 50 °C.

NH_4^+-exchanged zeolites (*i.e.* the amount of NH_4^+ ions released to the solution) and their activity in HMF conversion (see space-time yields in Table 1). The second observation is that there is a reversible de-ammoniation reaction for the NH_4-BEA zeolite that is not apparently present (in the investigated range) for NH_4-MFI. As confirmation, measurements carried out under isothermal conditions for 160 minutes at 50 °C reveal that only the BEA zeolite was able to fully restore the initial NH_4^+ content (Fig. 2b). There is thus a clear difference in the behavior of BEA and MFI in terms of reversible de-ammoniation that is likely related to the different locations of the acid sites (demonstrated also with the FTIR data, Table 2) and to the "confinement" effect of the zeolitic cage. It is likely that the differences in the catalytic performances of these two samples are related to these different characteristics.

3.3 Siting of NH_4^+ ions and competitive adsorption of bases

Few literature data contain analysis of the local siting of ammonium ions, for which monodentate, bidentate, or tridentate structures might be formed (Scheme 1).[33,34]

For the sake of brevity, we will describe in detail only the profiles of the IR spectra recorded for the NH_4-BEA zeolite and remark only on the differences observed in the other samples. Zeolite BEA is characterized by two sets of perpendicular straight 12-MR channels, running along the [100] and [010] directions.

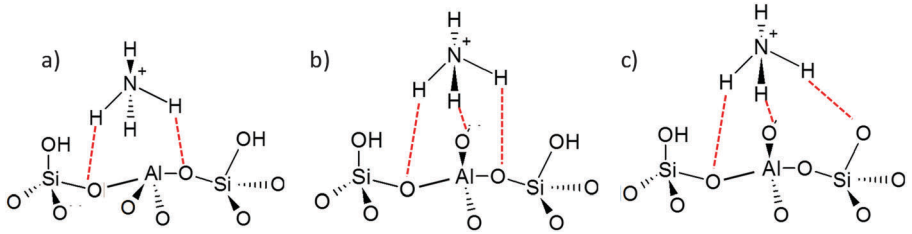

Scheme 1 Possible configurations of NH_4-zeolite bonding. (a) bidentate, (b) tridentate with C_{3v} symmetry, and (c) tridentate with C_s symmetry.

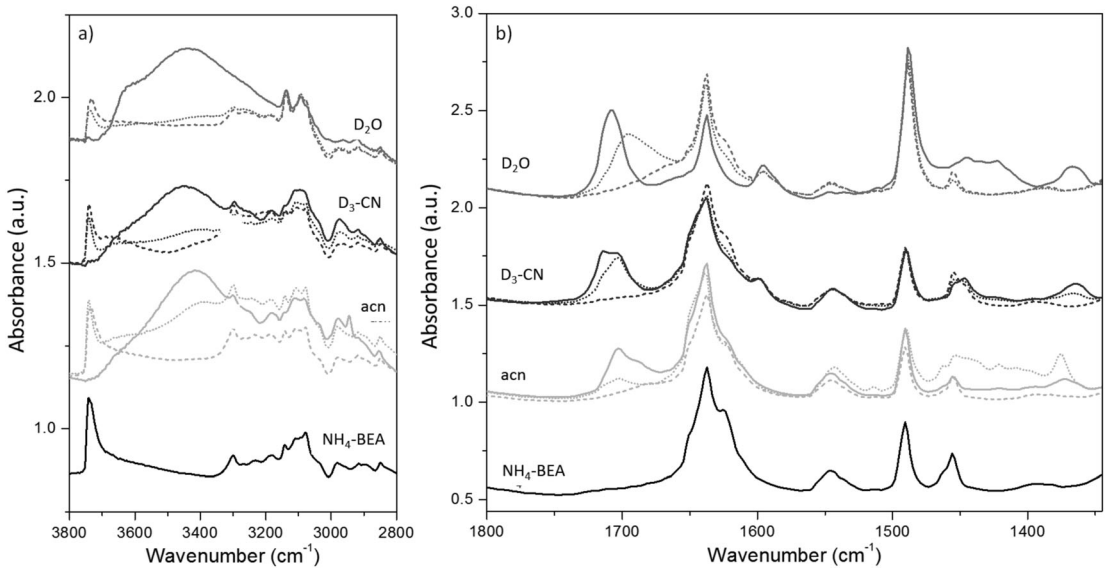

Fig. 3 FT-IR spectra of NH_4-BEA zeolite before and after base probe molecule adsorption (full lines), desorption at room temperature (dotted line) and at 150 °C (dashed line). (a) Hydroxyl region (b) NH_4^+ bending region.

They intersect in a third kind of curved channel along the [001] direction, whose geometry is governed by the stacking sequence, and create large cavities where bulky molecules can freely locate without causing a blockage.[35] BEA zeolites present high accessibility for all the directions of molecules up to a 5.95 Å diameter, thus also making it possible for bulky molecules to interact with all the acidic centers present in the catalyst.

Fig. 3 shows the IR spectra of the dehydrated parent NH_4-BEA after the dosage of different base probe molecules. The spectra were recorded after base saturation at room temperature (full line), evacuation at room temperature (dotted line) or at 150 °C under vacuum (dashed line).

NH_4-BEA displays an intensive 3745 cm^{-1} band in the OH stretching frequency region (Fig. 3a), related to isolated terminal SiOH groups located on the external and internal surfaces (low-frequency tail).[36] No feature at 3610 cm^{-1} is observed, due to the presence of NH_4^+ ions bonded to Brønsted acid centers. The broad and complex absorption covering the range 3300–2800 cm^{-1}, can be associated to stretching vibrations of N–H in different environments, *i.e.* monodentate, bidentate and tridentate hydrogen-bonded NH_4^+ configurations.[37] As also documented from *ab initio* calculations,[33,38] the negatively charged walls of the zeolites stabilize bidentate and tridentate structures. In agreement, we do not observe any absorption related to monodentate configurations, which usually present a steep feature at 3375 cm^{-1}. The dosage of the different base probes leads to the erosion of the bands associated with hydroxyl groups, and when further outgassing at room temperature is carried out, a full restoration of the starting configuration is achieved only for samples treated with acetonitriles. In the case of interaction with D_3-CN, the restoration of the silanol band is partially impeded by the formation of Si-OD species (band at 2757 cm^{-1}, not shown here). This effect is more pronounced upon dosage of D_2O.

We may suggest that this is direct proof of a change in the interaction status of NH_4^+ ions. In the 1800–1350 cm^{-1} frequency region, it is possible to identify the presence of two groups of IR-active bending modes: a triplet of peaks between 1550 and 1400 cm^{-1} associated to bidentate NH_4^+ species (which have two NH groups involved in H bonding, and hence have a C_{2v} symmetry), and an intense triplet in the range 1700–1600 cm^{-1}, typical of tridentate species (having three NH groups H-linked to the zeolite and a single unperturbed NH, with the symmetry C_{3v} or C_s, depending on the position of the oxygen to which the third H is linked). The free NH groups point into the channels and cavities and are not appreciably perturbed by the interaction with the opposite walls.

The interaction of NH_4-BEA with each base probe molecule deserves an individual explanation (Fig. 3b). The IR spectra obtained after interaction with acetonitrile (pK_a = 25) display a broad adsorption band centered at around 1700 cm^{-1} with a right shoulder, and another one appears at 1350 cm^{-1}. During evacuation at room temperature and 150 °C, these bands are eroded until the initial spectrum is completely restored. The profiles obtained with D_3-CN are similar to those previously described. The situation upon D_2O (pK_a = 16.6) dosage is different: saturation leads to the appearance of an intense band at 1700 cm^{-1}, which is removed during outgassing, but the features related to the tridentate species decrease in intensity (triplet), with a corresponding increase of a band at *ca.* 1590 cm^{-1}. In parallel, the band at 1550 cm^{-1} is irreversibly eroded and the peak at 1490 cm^{-1} doubles in intensity. Finally, the band at 1450 cm^{-1} is highly perturbed, but fully restored, upon outgassing at room temperature. The final spectrum obtained after outgassing at 150 °C reveals an overall decrease of the features related to tridentate species, and an increase of those typical of bidentate species, with a modification in the relative intensities after interaction with D_2O.

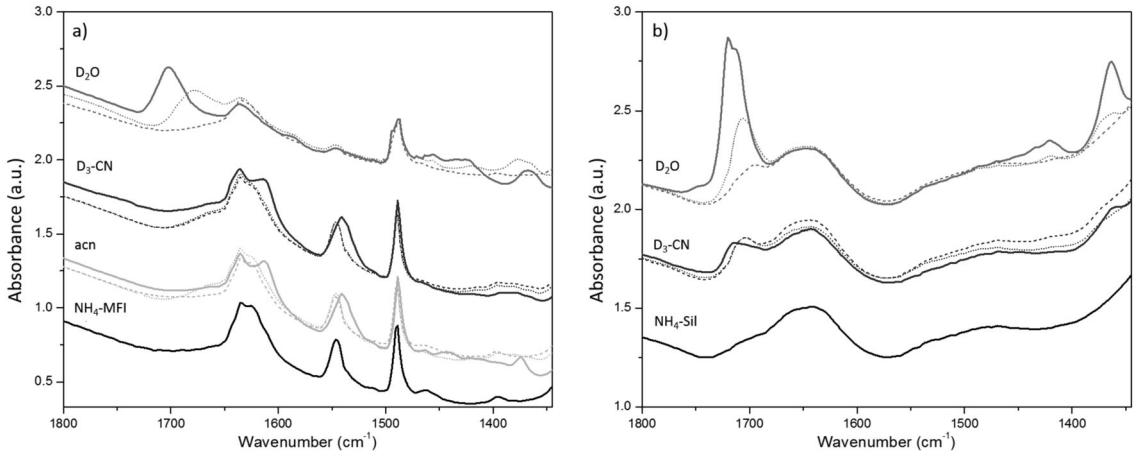

Fig. 4 FT-IR spectra of (a) NH_4-MFI and (b) NH_4-Sil samples before and after base probe molecule adsorption (full lines), desorption at room temperature (dotted line) and at 150 °C (dashed line) in the NH_4^+ bending region.

The same experiments carried out over the NH_4-MFI zeolite (Fig. 4a) reveal two substantial differences, with respect to the observations for NH_4-BEA.

Whereas in this case it is also possible to clearly observe the typical features of both bidendate and tridentate-bonded NH_4^+ species in the starting materials, the interactions of both acetonitrile and D_3-CN lead to a red-shift perturbation of the bands at 1620 and 1550 cm^{-1}, with a full recovery upon degassing at room temperature. This would suggest a higher instability of the two configurations, even in the presence of a very weak base. This behavior is even more pronounced in the presence of D_2O, where an overall attenuation of the bands (both of bidentate and tridentate species) is registered, as a proof of an irreversible reduction in the amount of NH_4^+ ions interacting with acidic Brønsted centers.

In the case of the NH_4-Sil sample (Fig. 4b), the features related to NH_4^+ species in different environments cannot be envisaged, probably due to their concentrations being below the detection limits. All these observations are direct proof of the strength of the NH_4^+ interaction with acidic centers, which in turn has been highlighted during the monitoring of NH_4^+ release in aqueous solution (Fig. 2).

4. Conclusions

BEA, MFI and Silicalite-1 zeolites in the ammonium and protonic forms have been tested in the etherification of HMF in anhydrous ethanol. The study of the sample acidity confirms that the selectivity to EMF and EOP is driven by the different natures and amounts of Lewis and Brønsted acid sites, respectively. In particular, the ammonium-exchanged form of zeolites presents a higher selectivity in comparison with the corresponding protonic form. The ammonium-exchanged form of the zeolite is active in the acid-catalyzed etherification reaction of HMF in anhydrous ethanol, leading to an improved selectivity and activity, in particular for the BEA zeolite form. The behavior is not related to ammonia dissociation in solution, but is likely associated to a reversible dissociation, which is favored by the BEA zeolite structure. FTIR data for NH_4^+ siting and shift by competitive adsorption reveal a significant difference between the BEA and MFI forms.

Although further studies are necessary to better understand this complex chemistry related to the dissociation of ammonium ions in solution, its dependence on the zeolite structure and the relationship between these phenomena and the catalytic behavior, we may conclude that the FTIR data for the characterization of these species and their stability, release of ammonia in solution and catalytic behavior are consistent.

We demonstrate for the first time that ammonium-exchanged zeolites are active and show better performances (particularly BEA) in acid-catalyzed etherification reactions. A critical condition is that dissociated ammonia remains in the zeolite cages and may be reversible re-adsorbed. Thus it is likely that the dissociated ammonia participates in the reaction or induces a confinement effect. The exact nature of these aspects is under further investigation.

In conclusion, the relation of the reversible dissociation of NH_4^+ ions in the zeolite intra-cages with the zeolite structure itself is responsible for the different catalytic reactivity of the samples, and may lead to the better performances with respect to the corresponding protonic form. This has been demonstrated for the HMF etherification with ethanol, a reaction of industrial interest for the production of bio-diesel additives. However, it is likely of more general relevance to understand the catalytic chemistry of zeolites in these types of reactions and the possibility of enhancing the behavior by cooperative effects.

References

1 A. Corma, *Chem. Rev.*, 1997, **97**, 2373–2420.
2 J. Čejka, G. Centi, J. Perez-Pariente and W. J. Roth, *Catal. Today*, 2012, **179**, 2–15.
3 L. Wang and F.-S. Xiao, *Green Chem.*, 2015, **17**, 24–39.
4 D. Kubicka and O. Kikhtyanin, *Catal. Today*, 2015, **243**, 10–22.
5 P. A. Jacobs, M. Dusselier and B. F. Sels, *Angew. Chem., Int. Ed.*, 2014, **53**, 8621–8626.

6 P. Lanzafame, D. M. Temi, S. Perathoner, A. N. Spadaro and G. Centi, *Catal. Today*, 2012, **179**, 178–184.
7 A. A. Lappas, S. Bezergianni and I. A. Vasalos, *Catal. Today*, 2009, **145**, 55–66.
8 M. M. Antunes, S. Lima, P. Neves, A. L. Magalhães, E. Fazio, A. Fernandes, F. Neri, C. M. Silva, S. M. Rocha, M. F. Ribeiro, M. Pillinger, A. Urakawa and A. A. Valente, *J. Catal.*, 2015, **329**, 522–537.
9 K. S. Arias, S. I. Al-Resayes, M. J. Climent, A. Corma and S. Iborra, *ChemSusChem*, 2013, **6**, 123–131.
10 K. S. Arias, M. J. Climent, A. Corma and S. Iborra, *ChemSusChem*, 2014, **7**, 210–220.
11 J. Faria, M. Pilar Ruiz and D. E. Resasco, *ACS Catal.*, 2015, **5**, 4761–4771.
12 J. Jae, G. A. Tompsett, A. J. Foster, K. D. Hammond, S. M. Auerbach, R. F. Lobo and G. W. Huber, *J. Catal.*, 2011, **279**, 257–268.
13 J. S. Kruger, V. Choudhary, V. Nikolakis and D. G. Vlachos, *ACS Catal.*, 2013, **3**, 1279–1291.
14 E. Taarning, C. M. Osmundsen, X. Yang, B. Voss, S. I. Andersen and C. H. Christensen, *Energy Environ. Sci.*, 2011, **4**, 793–804.
15 B. Kamm, *Angew. Chem., Int. Ed.*, 2007, **46**, 5056–5058.
16 P. Lanzafame, G. Centi and S. Perathoner, *Catal. Today*, 2014, **234**, 2–12.
17 S. Abate, P. Lanzafame, S. Perathoner and G. Centi, *ChemSusChem*, 2015, **8**, 2854–2866.
18 G. Centi, P. Lanzafame and S. Perathoner, *Catal. Today*, 2011, **167**, 14–30.
19 S. Abate, K. Barbera, G. Centi, P. Lanzafame and S. Perathoner, *Catal. Sci. Technol.*, 2016, DOI: 10.1039/C5CY02184G.
20 P. Lanzafame, D. M. Temi, S. Perathoner, G. Centi, A. Macario, A. Aloise and G. Giordano, *Catal. Today*, 2011, **175**, 435–441.
21 K. Barbera, P. Lanzafame, A. Pistone, S. Millesi, G. Malandrino, A. Gulino, S. Perathoner and G. Centi, *J. Catal.*, 2015, **323**, 19–32.
22 P. Lanzafame, K. Barbera, S. Perathoner, G. Centi, A. Aloise, M. Migliori, A. Macario, J. B. Nagy and G. Giordano, *J. Catal.*, 2015, **330**, 558–568.
23 E. Catizzone, A. Aloise, M. Migliori and G. Giordano, *Appl. Catal., A*, 2015, **502**, 215–220.
24 B. P. Pinto, J. T. de Lyra, J. A. C. Nascimento and C. J. A. Mota, *Fuel*, 2016, **168**, 76–80.
25 A. Bohre, B. Saha and M. M. Abu-Omar, *ChemSusChem*, 2015, **8**, 4022–4029.
26 R. J. van Putten, J. C. van der Waal, E. de Jong, C. B. Rasrendra, H. J. Heeres and J. G. de Vries, *Chem. Rev.*, 2013, **113**, 1499–1597.
27 J. Luo, J. Yu, R. J. Gorte, E. Mahmoud, D. G. Vlachos and M. A. Smith, *Catal. Sci. Technol.*, 2014, **4**, 3074–3081.
28 A. Comas-Vives, M. Valla, C. Coperet and P. Sautet, *ACS Cent. Sci.*, 2015, **1**, 313–319.
29 A. J. Jones, R. T. Carr, S. I. Zones and E. Iglesia, *J. Catal.*, 2014, **312**, 58–68.
30 A. J. Jones, S. I. Zones and E. Iglesia, *J. Phys. Chem. C*, 2014, **118**, 17787–17800.
31 E. Kassab, J. Fouquet, M. Allavena and E. M. Evleth, *J. Phys. Chem.*, 1993, **97**, 9034–9039.
32 J. Jiou, K. Chiravuri, A. Gudapati and J. J. Gassensmith, *Curr. Org. Chem.*, 2014, **18**, 2002–2009.
33 A. Zecchina, L. Marchese, S. Bordiga, C. Pazè and E. Gianotti, *J. Phys. Chem. B*, 1997, **101**, 10128–10135.
34 W. Wu and E. Weitz, *Appl. Surf. Sci.*, 2014, **316**, 405–415.
35 R. Buzzoni, S. Bordiga, G. Ricchiardi, C. Lamberti and A. Zecchina, *Langmuir*, 1996, **12**, 930–940.
36 K. Barbera, F. Bonino, S. Bordiga, T. V. W. Janssens and P. Beato, *J. Catal.*, 2011, **280**, 196–205.
37 K. Suzuchi, T. Noda, N. Katada and M. Niwa, *J. Catal.*, 2007, **250**, 151–160.
38 E. H. Teunissen, R. A. van Santen, A. P. J. Jansen and F. B. van Duijneveldt, *J. Phys. Chem.*, 1993, **97**, 203–210.